Supporting Information

Hierarchical Tri-functional Electrocatalysts Derived from Bimetallic-imidazolate Framework for Overall Water Splitting and Rechargeable Zinc-air Batteries

Sung Hoon Ahn[a,b], *and Arumugam Manthiram* [a,*]

a Materials Science and Engineering Program & Texas Materials Institute
The University of Texas at Austin, Austin, Texas, 78712, United States
b Department of Bio-chemical and Polymer Engineering
Chosun University, Gwangju, 501-759, Republic of Korea

Characterizations

X-ray diffraction (XRD) patterns were recorded on a Rigaku MiniFlex 600 with Cu Kα radiation. Thin-film XRD patterns were obtained on an Empyrean equipment with Cu Kα radiation. Fourier-transform infrared spectroscopy (FT-IR) spectra were recorded on a FT-IR spectrometer (Nicolet iS5). Field emission scanning electron microscopy (FE-SEM) images were obtained with a FEI Quanta 650 FE-SEM. Transmission electron microscopy (TEM) and high resolution TEM (HRTEM) images and elemental mapping analysis were carried out with a JEOL 2010F TEM. X-ray photoelectron spectra (XPS) were obtained with a Kratos Axis Ultra DLD with Al Kα (1486.6 eV) X-ray source. Porosity analysis was performed with an automated gas sorption apparatus (AutoSorb iQ2, Quantachrome). Textural properties such as the specific surface area, pore volume, and pore size distribution were estimated from each corresponding N_2 adsorption−desorption isotherm with the Brunauer − Emmett – Teller (BET) equation and quenched solid density functional theory (QSDFT) model for slit shaped, spherical, and cylindrical pores. The nickel and cobalt contents were measured with an inductively coupled plasma (ICP) analyzer (Agilent 7700).

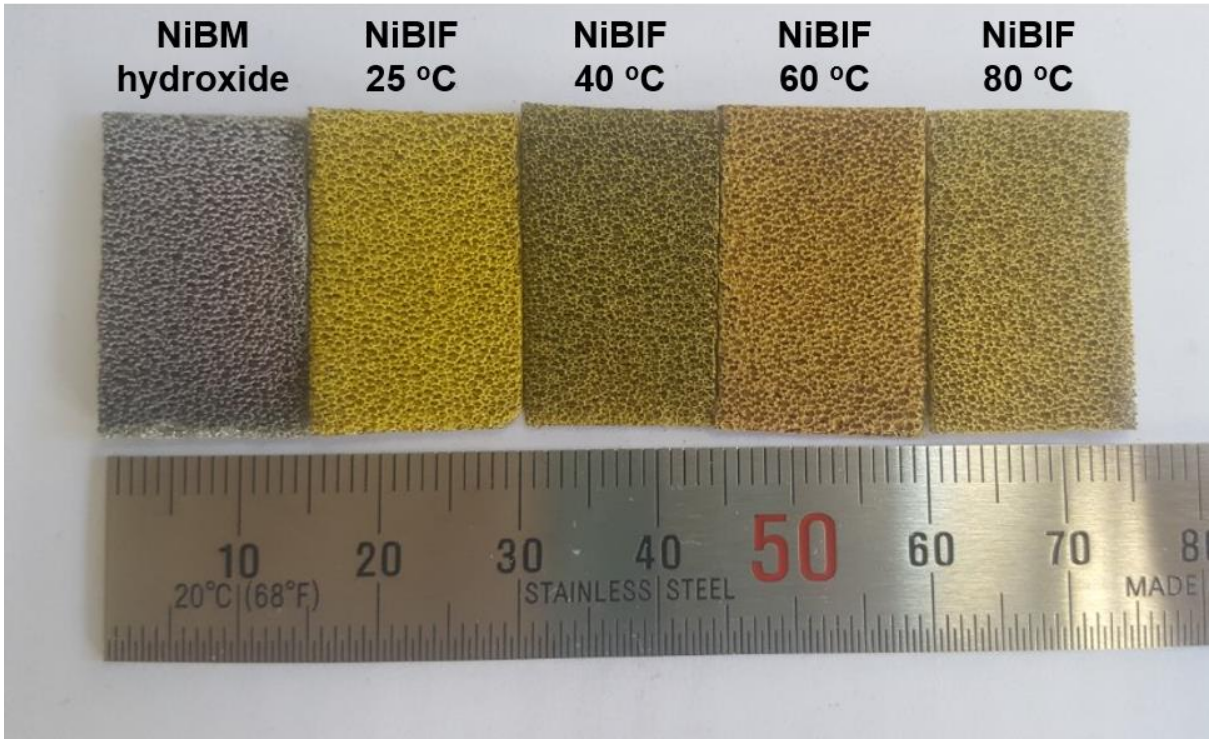

Figure S1. Picture of nickel-rich bimetallic hydroxide (NiBM hydroxide) and nickel-rich bimetallic imidazolate framework (NiBIF) converted from NiBM in 2-methylimidazole aqueous solution at 25, 40, 60 and 80 °C for 12 h.

Figure S2. Picture of ZIF-67/NiF (left) and NiBIF/NiF (right) that were processed at 60 °C for 12 h.

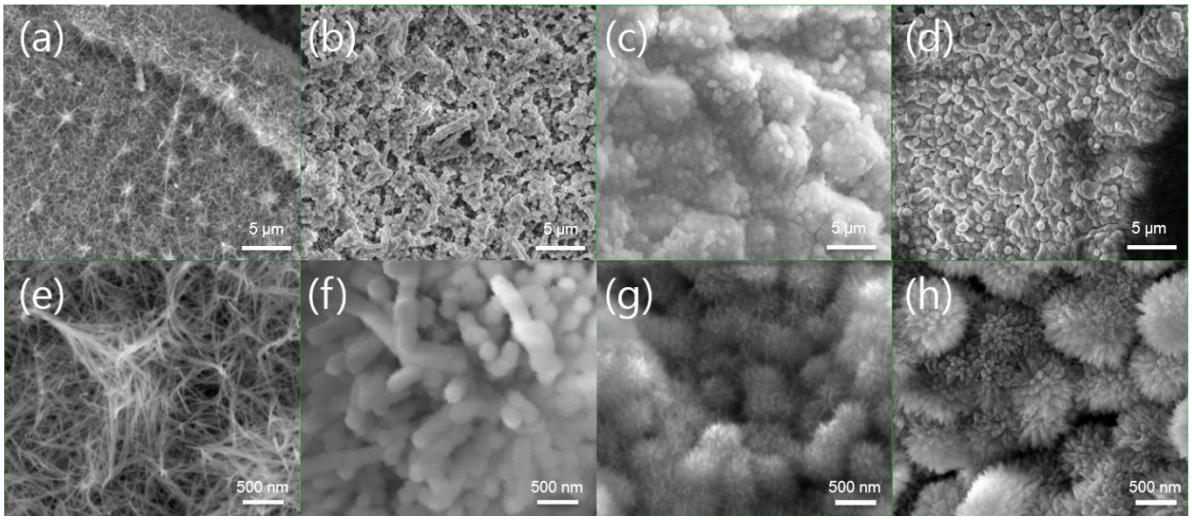

Figure S3. FE-SEM images of (a,e) bimetallic hydroxide nanowires (NiBM hydroxide), and the nickel-rich bimetallic imidazolate framework (NiBIF) converted from NiBM nanostructures in 2-methylimidazole aqueous solution at (b,e) 25 ºC, (c,g) 40 ºC, and (d,h) 50 ºC for 8 h.

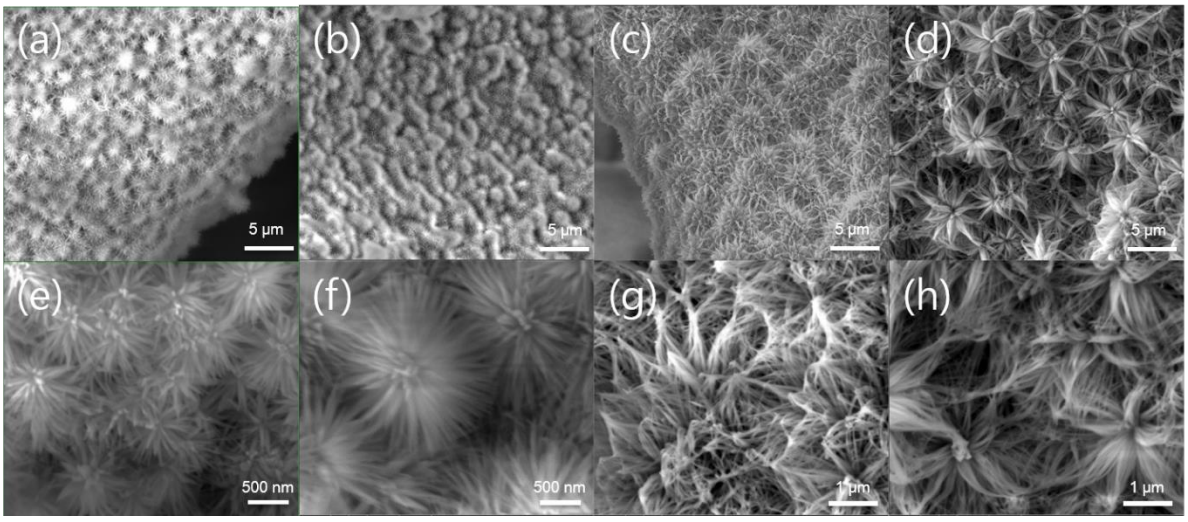

Figure S4. FE-SEM images of NiBIF converted from NiBM hydroxide in 2-methylimidazole aqueous solution at (a,e) 60 ºC, (b,f) 70 ºC, (c,g) 80 ºC, and (d,h) 90 ºC for 8 h.

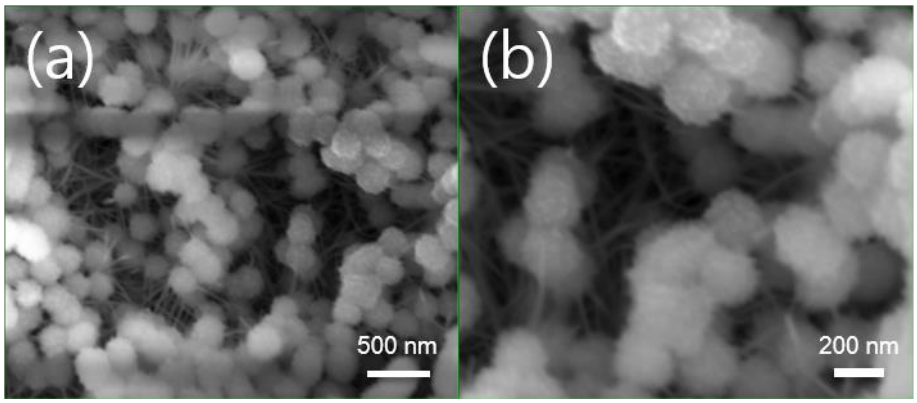

Figure S5. FE-SEM images of NiBIF processed at 25 ºC for 12 h, in the other area from Figure S3b and e.

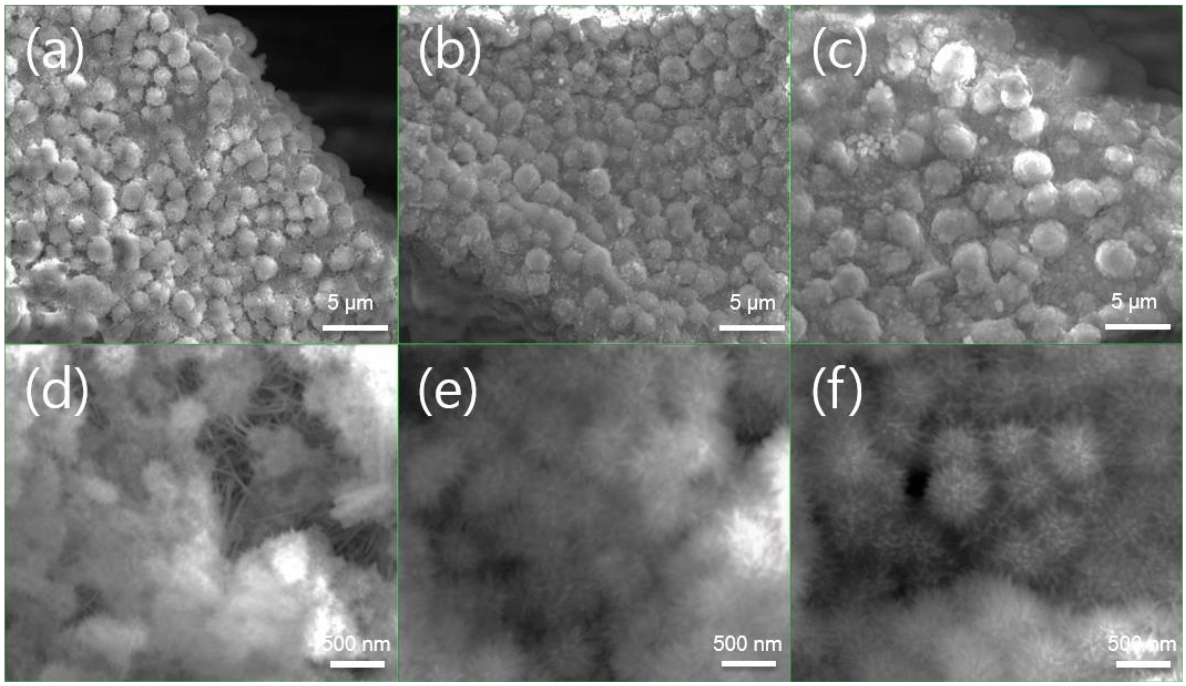

Figure S6. FE-SEM images of NiBIF processed at 40 ºC for (a,d) 2 h, (b,e) 4 h, and (c,e) 8 h.

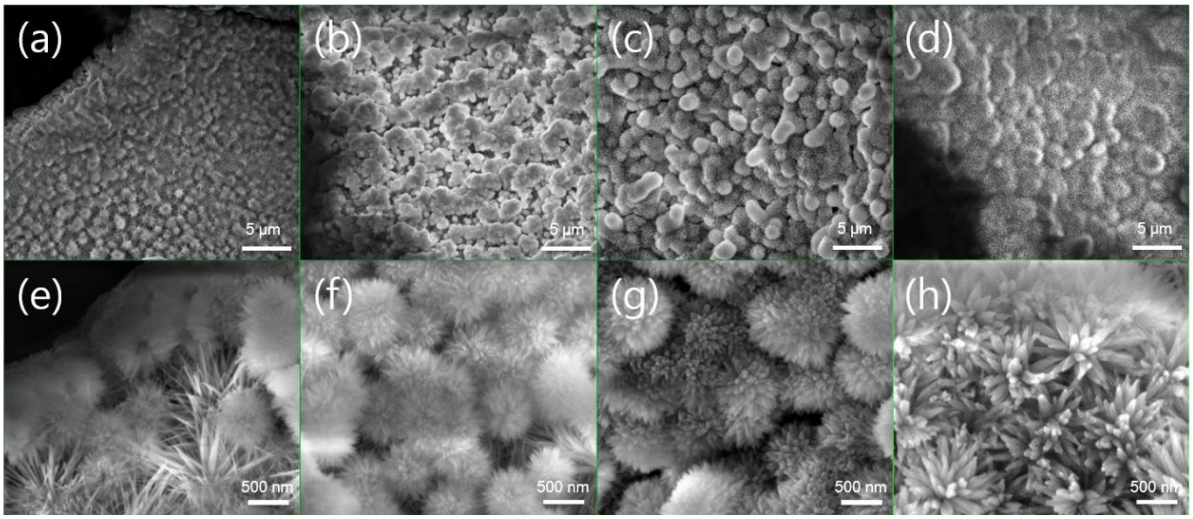

Figure S7. FE-SEM images of NiBIF processed at 50 ºC for(a,e) 2 h, (b,e) 4 h, (c,e) 8 h, and (d, e) 12 h.

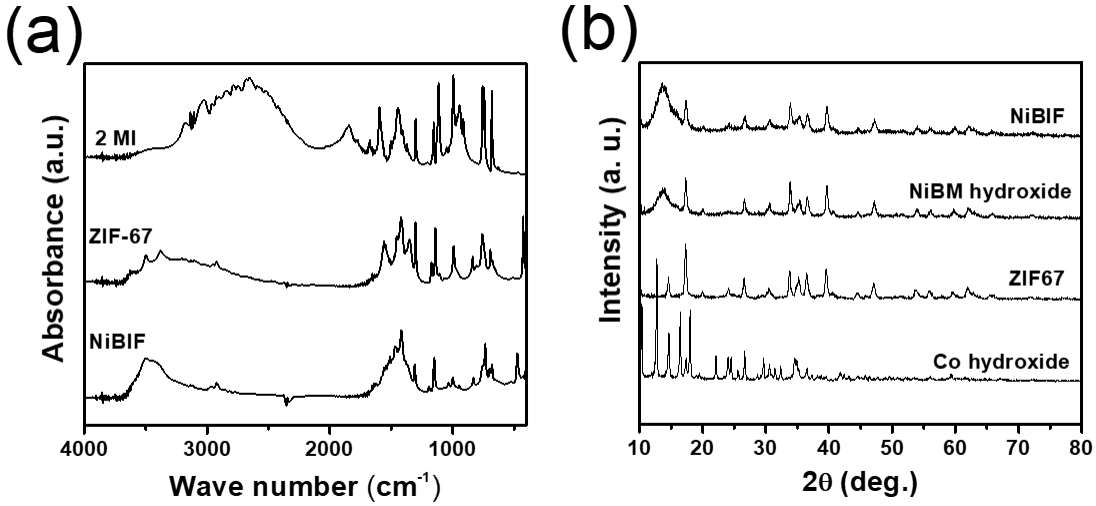

Figure S8. (a) FT-IR spectra of 2-methylimidazole, ZIF-67, and NiBIF. (b) XRD patterns of cobalt hydroxide, ZIF-67, nickel-rich bimetallic hydroxide (NiBM hydroxide), and NiBIF.

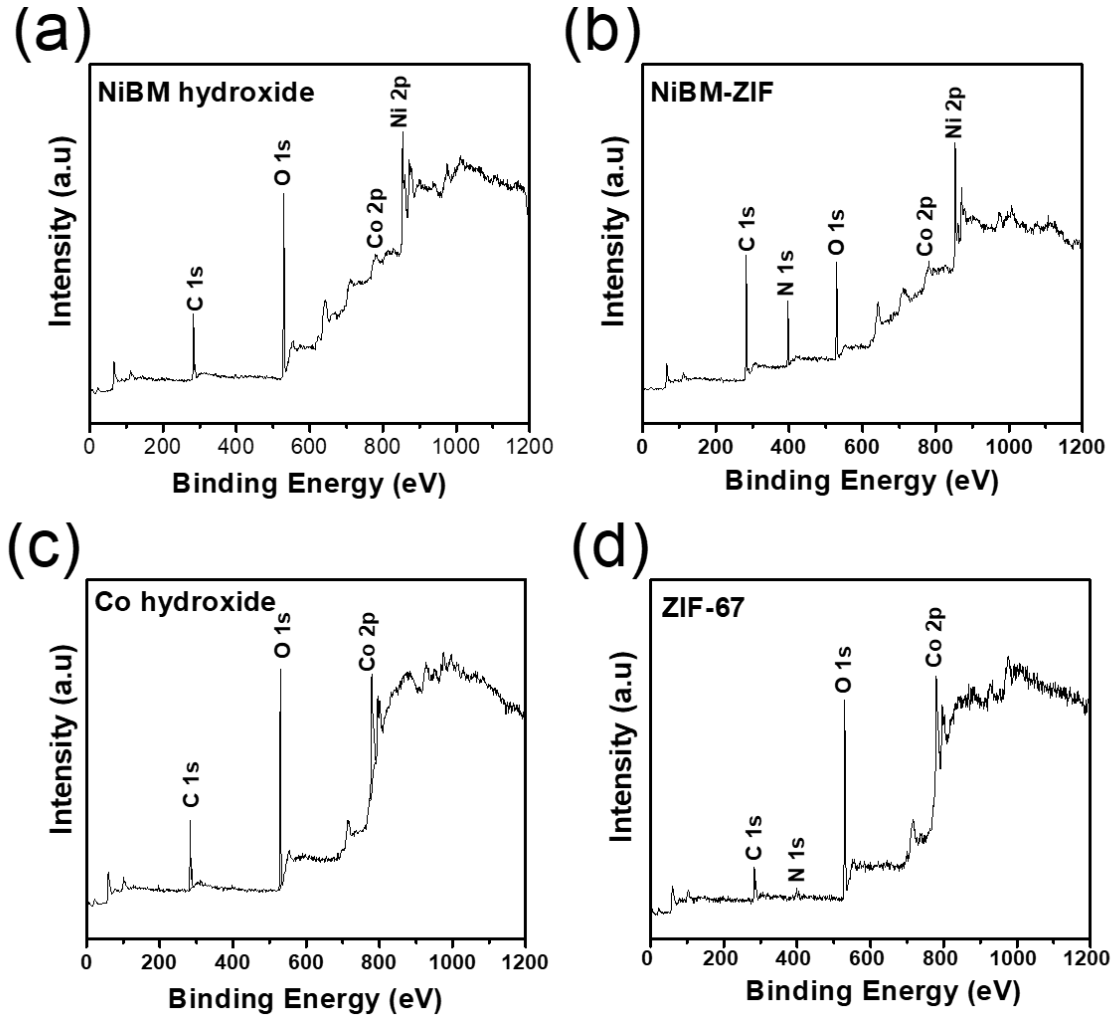

Figure S9. XPS survey spectra of (a) nickel-rich bimetallic hydroxide (NiBM hydroxide), (b) NiBIF, (c) Co hydroxide, and (d) ZIF-67.

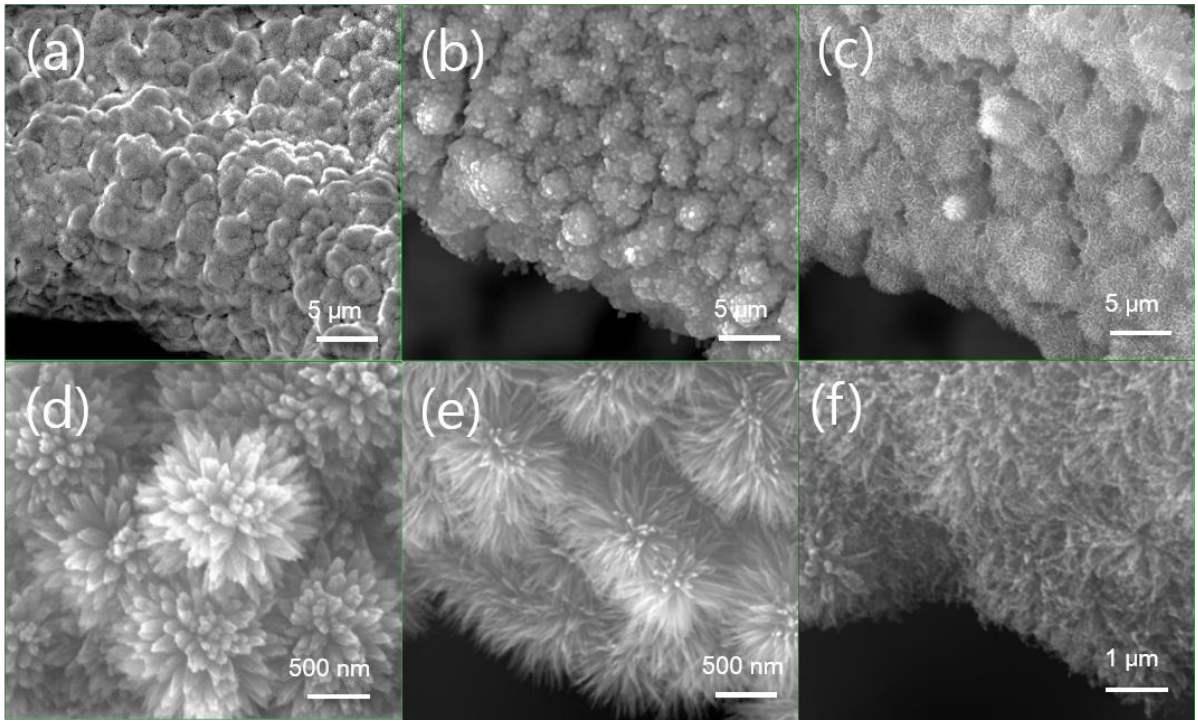

Figure S10. FE-SEM images of (a,c) NiBIF , (b),(e) NiBM@N_xC annealed at 350 ºC for 3 h, and (c,f) NiBM@N_xC after annealing process at 800 ºC for 3 h.

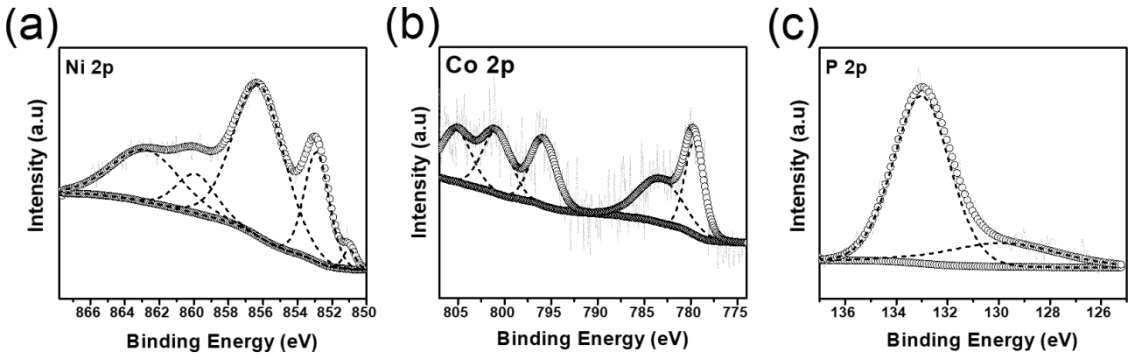

Figure S11. (a) Fine Ni 2p, (b) Co 2p, and (c) P 2p XPS spectra of NiBMP@N_xC.

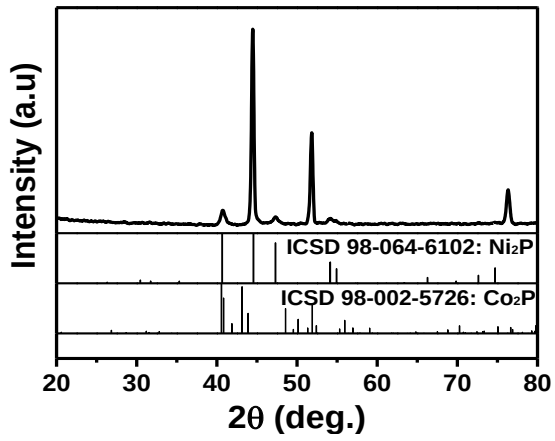

Figure S12. Thin-film XRD pattern of NiBMP@N_xC.

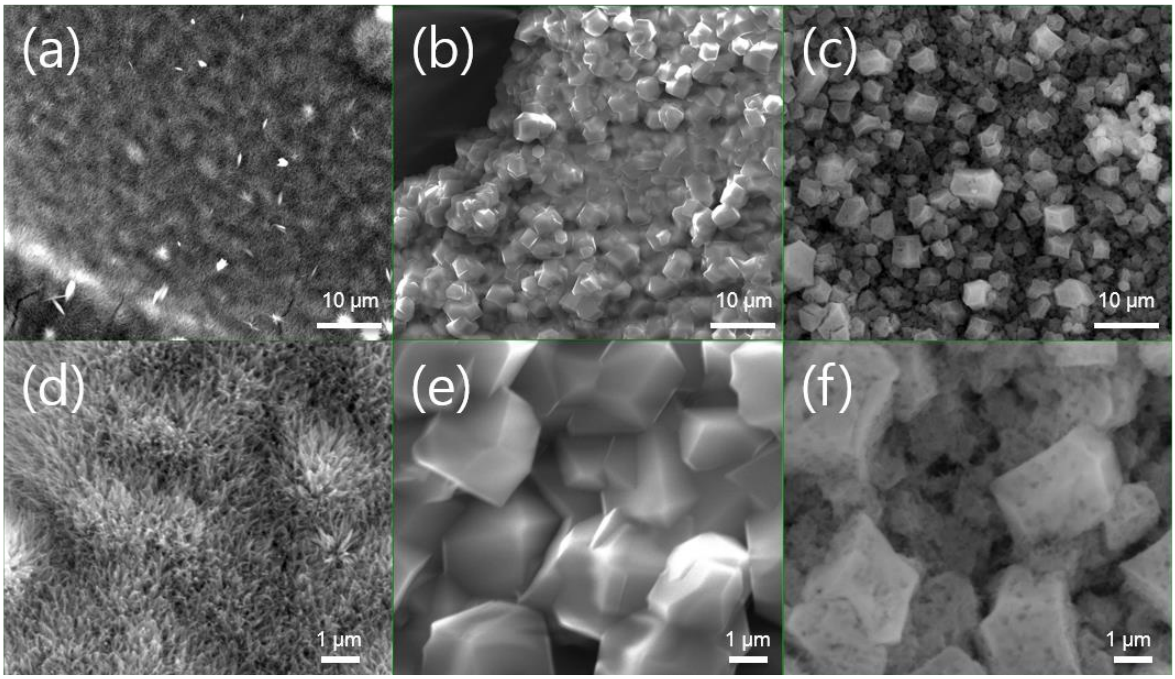

Figure S13. FE-SEM images of (a,d) Co hydroxide NWs, (b,e) ZIF-67, and (c,e) ZIF-67-P directly grown onto the nickel foam.

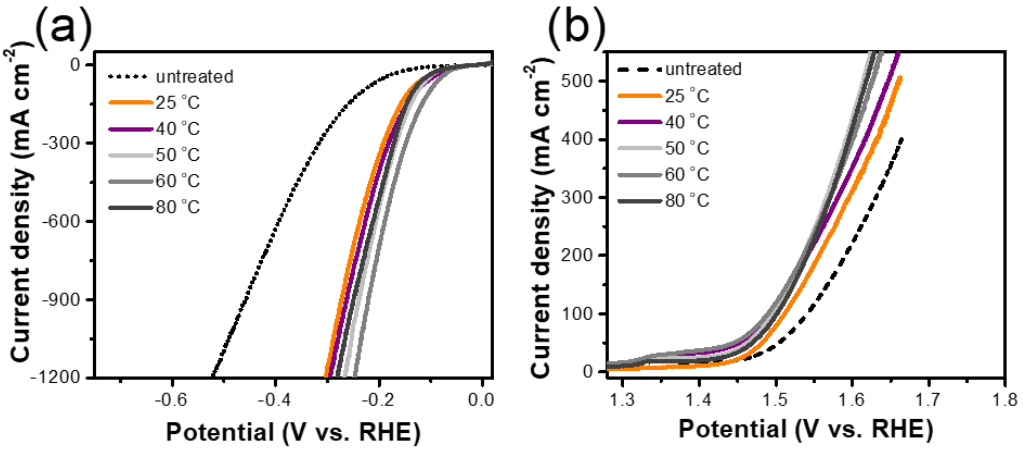

Figure S14. Polarization curves of various metal phosphide catalysts produced from untreated NiBM hydroxide (displayed as untreated) and NiBIF processed at 25, 40, 50, 60, 80 ºC with a scan rate at 2 mV s^{-1} in 1 M KOH toward (a) HER and (b) OER.

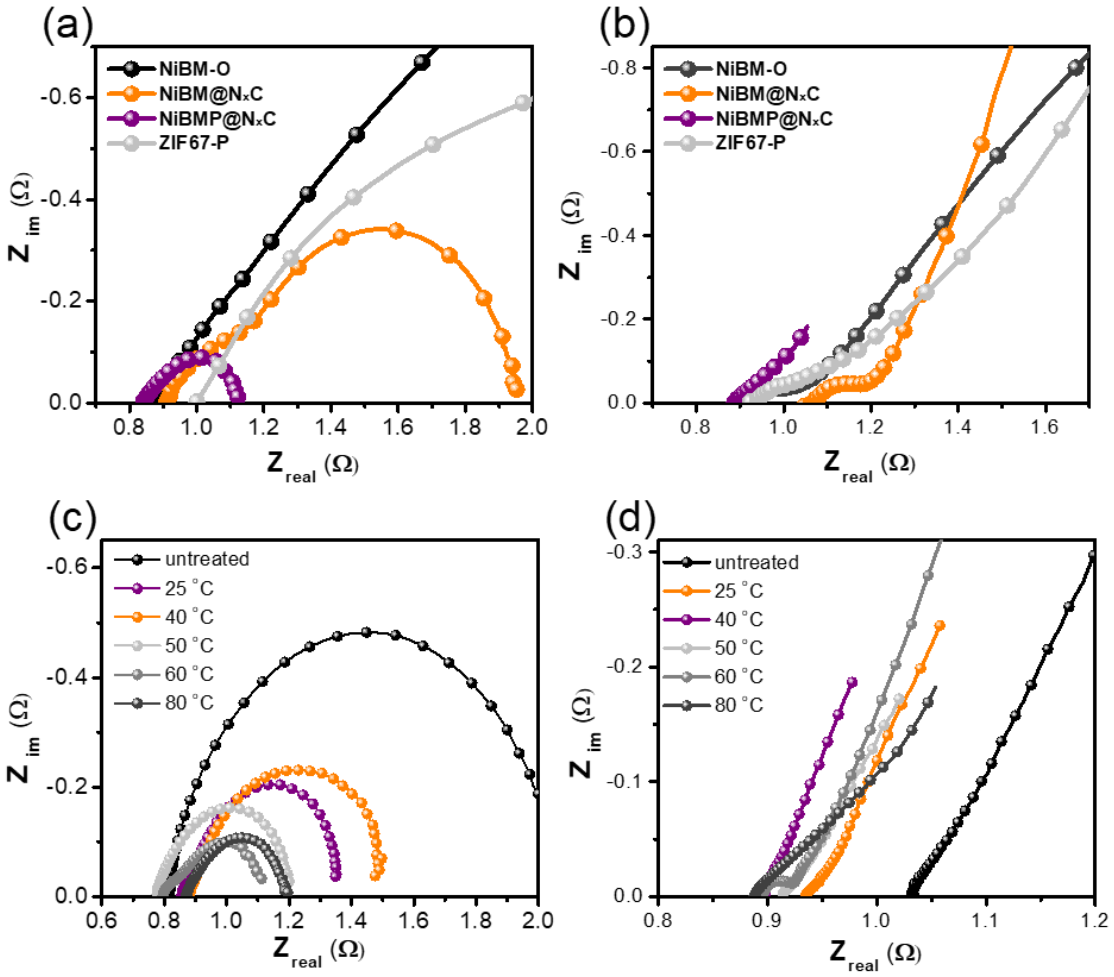

Figure S15. Nyquist plots of (a) NiBM-O, NiBM@N_xC, NiBMP@N_xC and ZIF67-P with an applied overpotential at 100 mV toward HER and (b) with an applied overpotential at 250 mV toward OER. (c) Nyquist plots of various metal phosphide catalysts produced from untreated NiBM hydroxide (displayed as untreated) and NiBIF processed at 25, 40, 50, 60, 80 ºC with an applied overpotential at 100 mV toward HER, (d) with an applied overpotential at 250 mV toward OER.

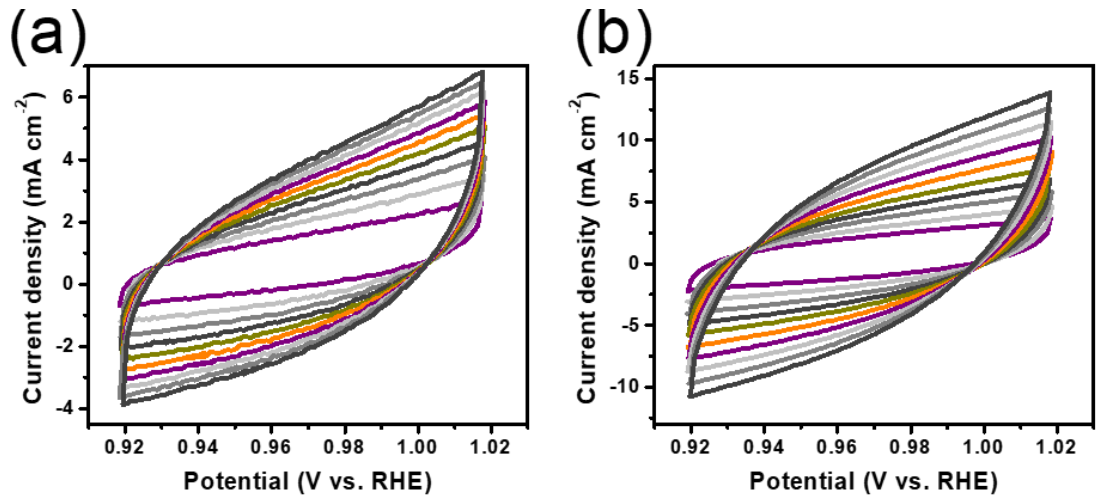

Figure S16. Cyclic voltammograms of (a) ZIF67-P and (b) NiBMP@N_xC recorded at various scan rates of 10, 20, 30, 40, 50, 60, 70, 80, 90 and 100 mV s^{-1}.

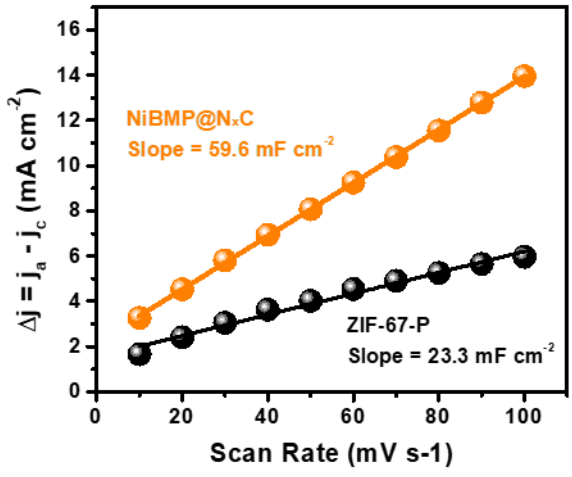

Figure S17. ΔJ (=Ja−Jc) of NiBMP@N_xC, ZIF67-P plotted against the scan rates.

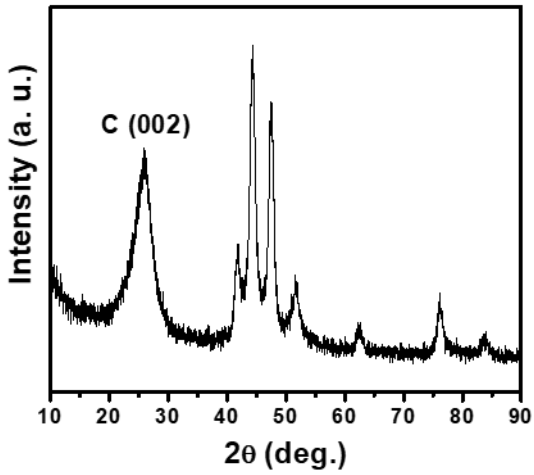

Figure S18. XRD pattern of NiBM@N_xC.

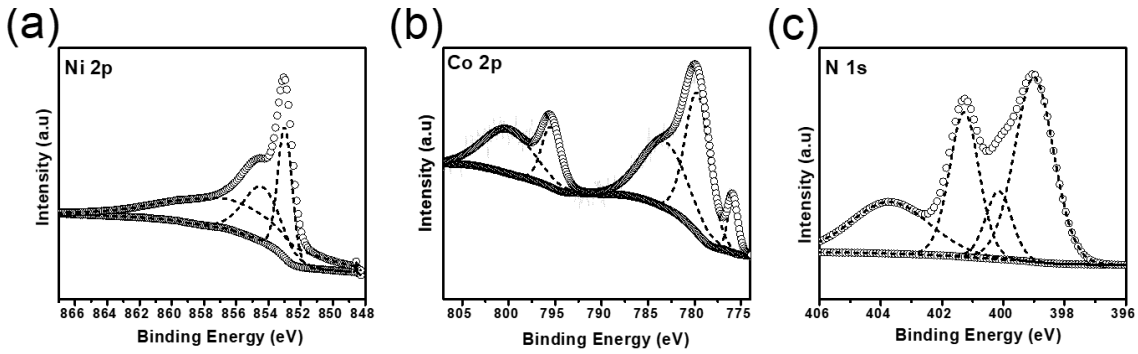

Figure S19. Fine (a) Ni 2p, (b) Co 2p, and (c) N 1s XPS spectra of NiBM@N_xC.

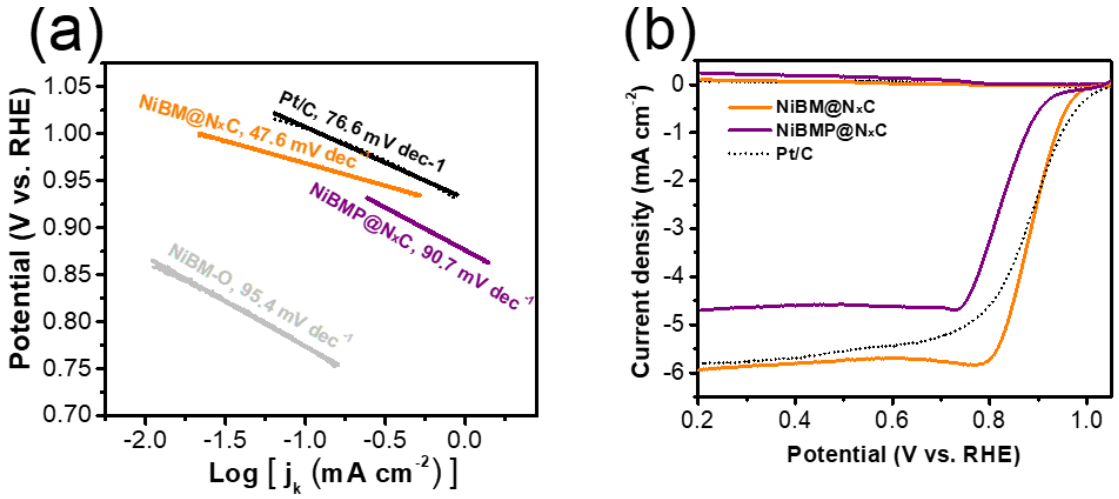

Figure S20. (a) Tafel plots derived from Figure 5b and (b) LSV curves obtained from rotating ring-disk experiments (RRDE) for NiBM@N_xC, NiBMP@N_xC catalysts and Pt/C catalyst in O_2-saturated 0.1 M KOH solution at 1600 rpm.

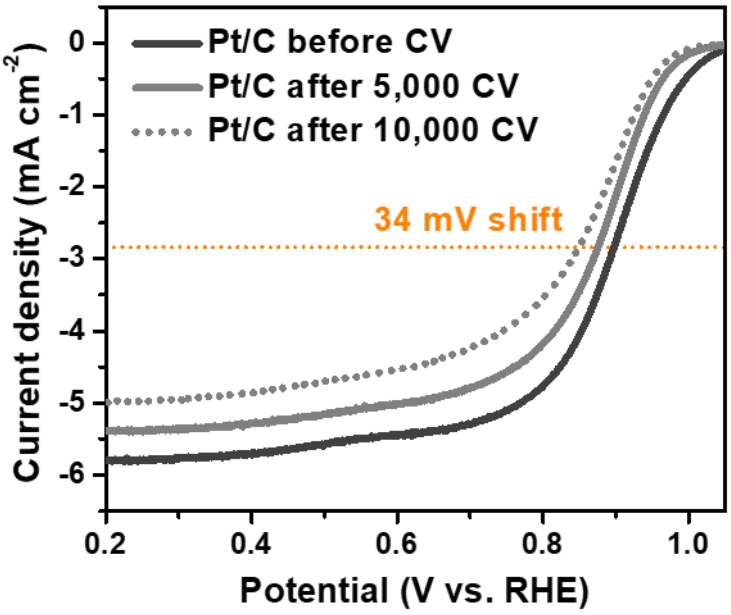

Figure S21. LSV curves of Pt/C catalyst before (dark gray line) and after 5,000 (gray line), cycles and after 10,000 cycles (dotted gray line) from 0.6 V_{RHE} to 1.0 V_{RHE} in N_2-saturated 0.1 M KOH electrolyte at 50 mV s^{-1}.

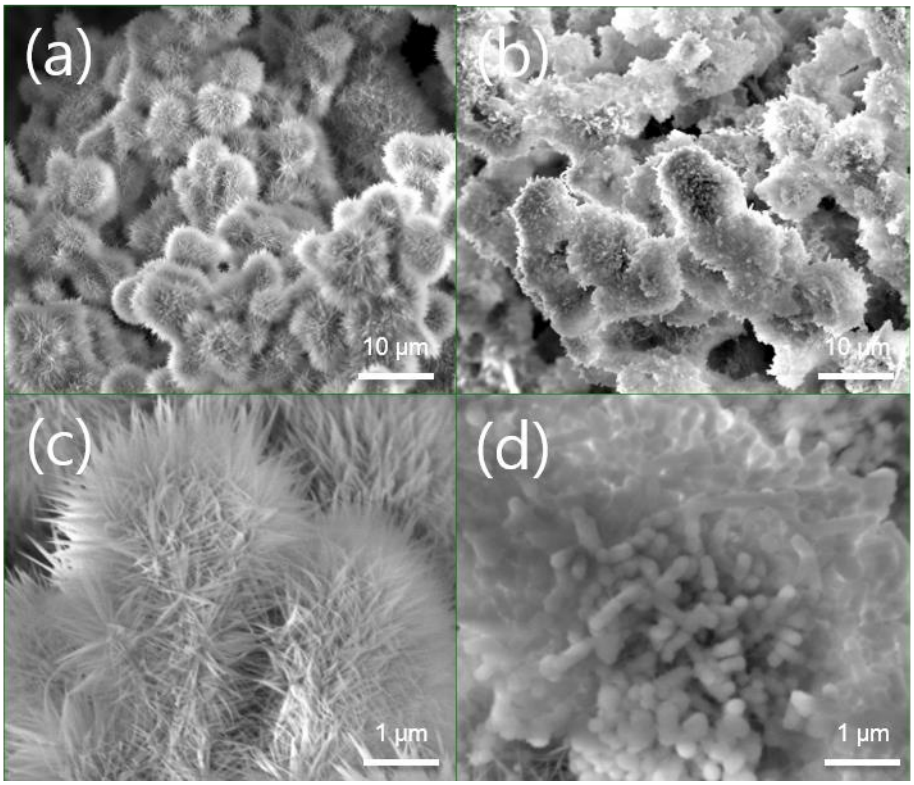

Figure S22. SEM images of (a,c) NiBM hydroxide precipitates and (b,d) NiBIF precipitates processed at 25 ºC for 12 h.

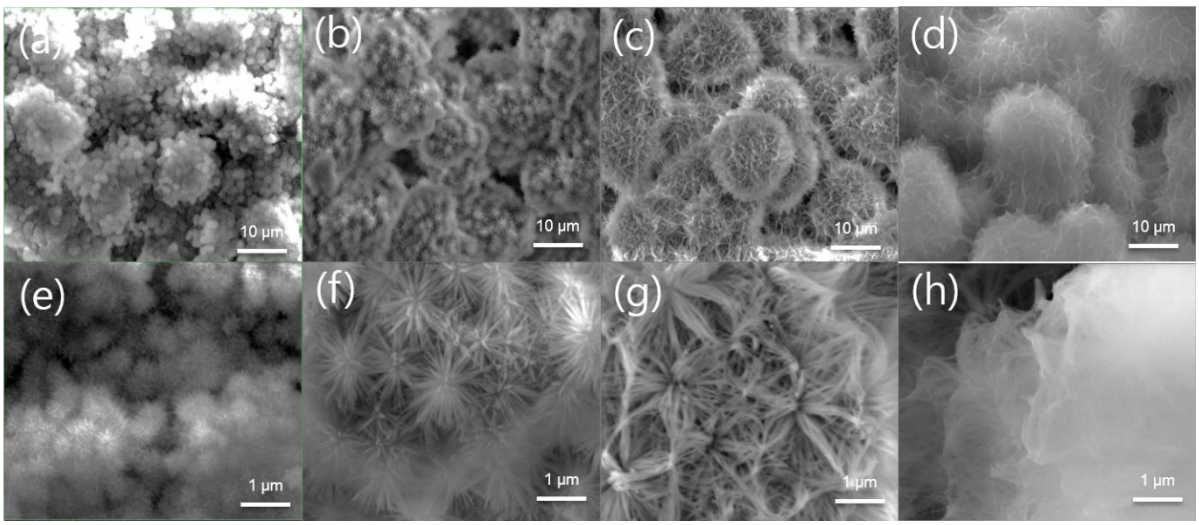

Figure S23. SEM images of NiBIF precipitates processed at (a,e) 40 ºC, (b,e) 50 ºC, (c),e) 60 ºC, (d,e) 80 ºC for 12 h.

Figure S24. Pictures of ZIF67 precipitates (left) and NiBIF precipitates (right). Both samples were processed at 60 ºC.

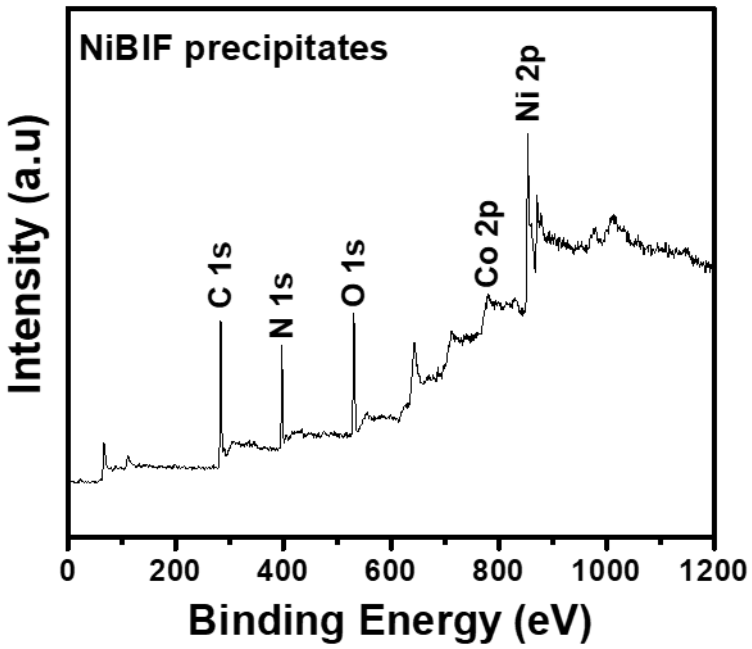

Figure S25. XPS spectra of NiBIF precipitates.

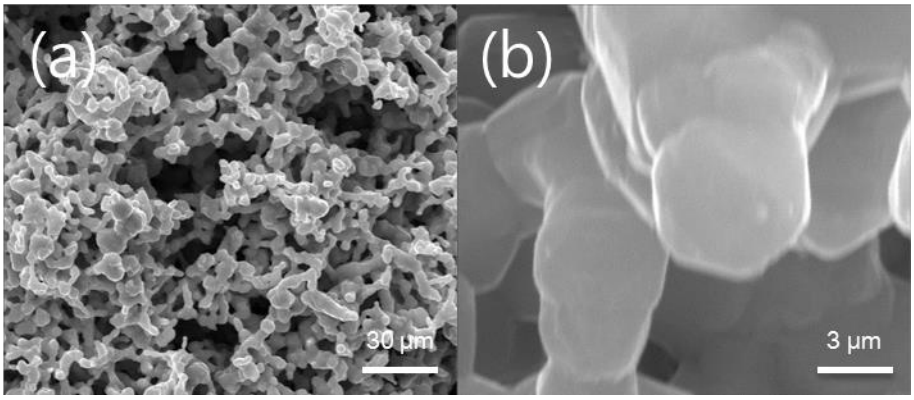

Figure S26. SEM images of nickel-rich bimetallic hydroxide (NiBM-hyodrixde) precipitates after the annealing process at 800 ºC for 3 h.

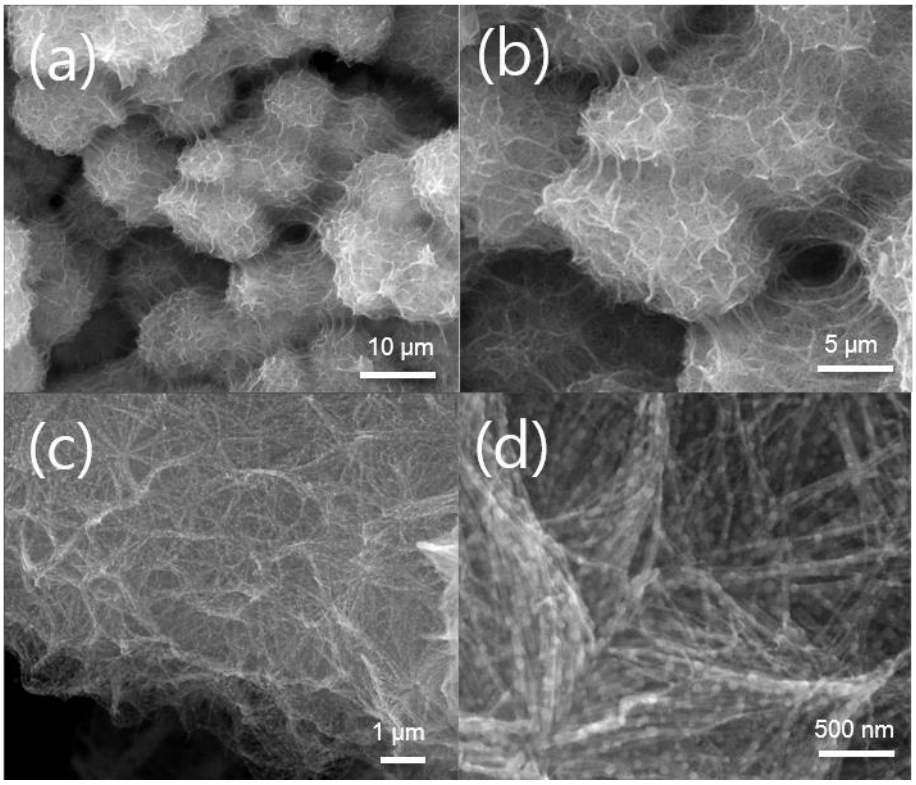

Figure S27. SEM images of NiBM@N_xC-80.

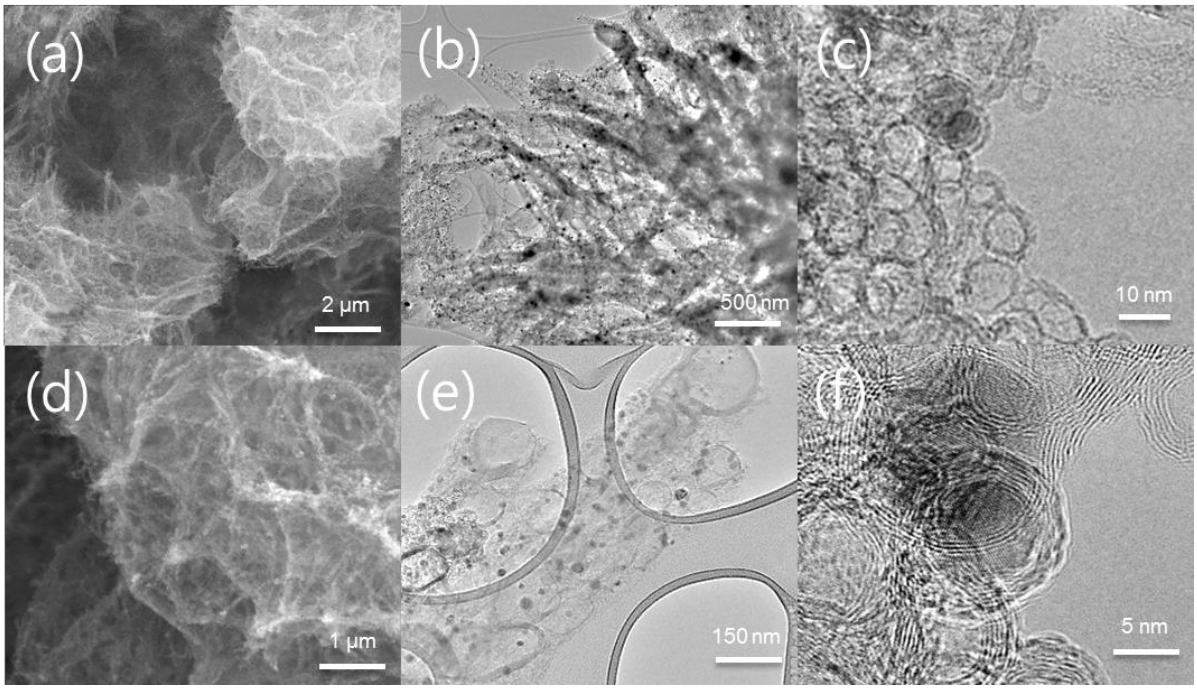

Figure S28. (a,d) SEM images, (b,e) TEM images, and (c,e) HR-TEM images of NiBM@N_xC-60.

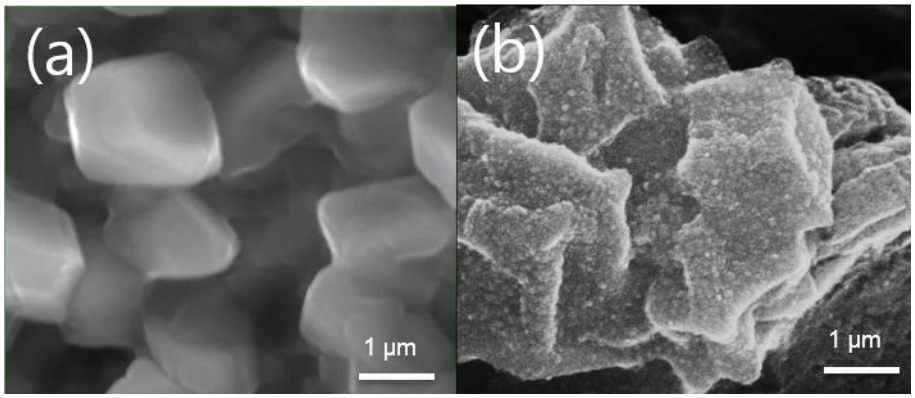

Figure S29. SEM images of (a) ZIF67 precipitates and (b) ZIF67@N_xC.

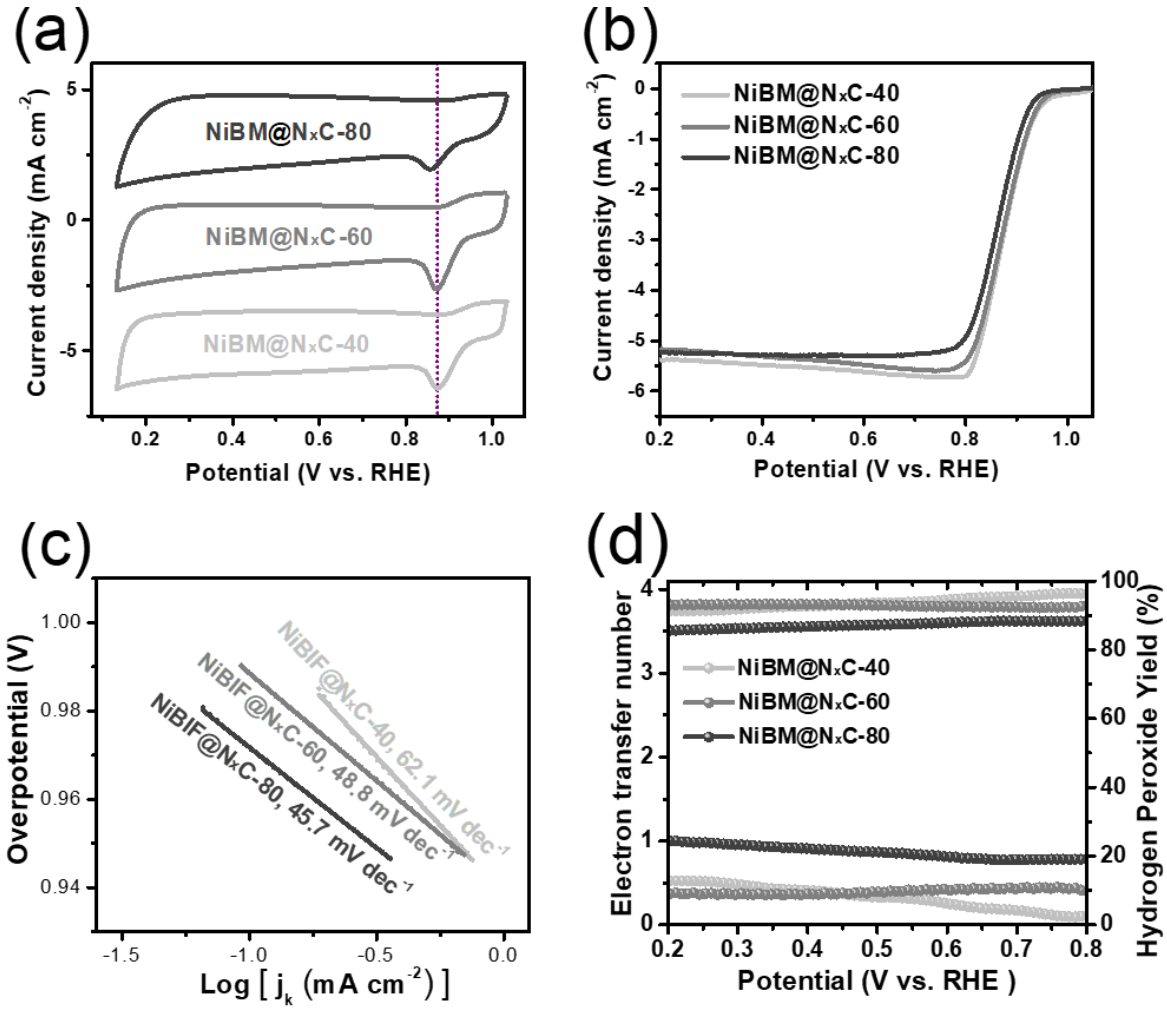

Figure S30. (a) CV curves of NiBM@N_xC samples in O_2 saturated 0.1 M KOH electrolyte. (b) LSV curves of the as-prepared NiBM@N_xC in O_2-saturated 0.1 M KOH electrolyte at a rotation speed of 1600 rpm, (c) Tafel plots from panel b, (d) peroxide yield and electron-transfer number of the NiBM@N_xC catalysts.

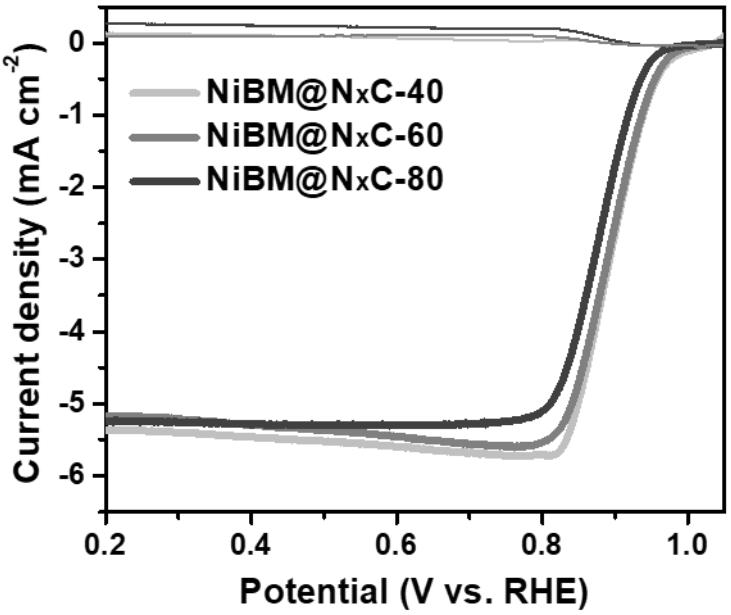

Figure S31. LSV curves obtained from rotation ring-disk experiments (RRDE) for as-prepared NiBM@N_xC catalysts and Pt/C catalyst in O_2-saturated 0.1 M KOH solution at 1600 rpm.

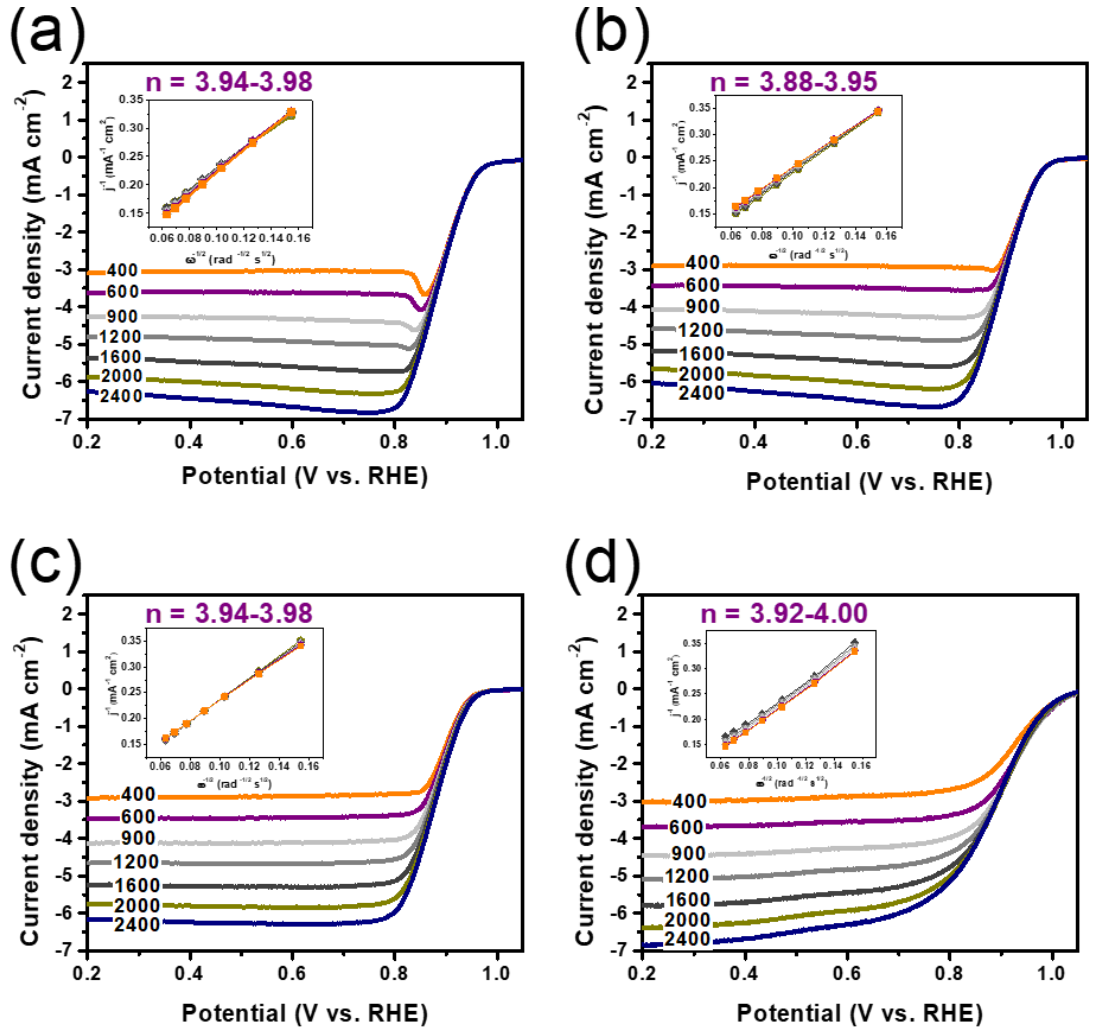

Figure S32. LSV curves of (a) NiBM@N_xC-40, (b) NiBM@N_xC-60, (c) (b) NiBM@N_xC-80, (d) Pt/C at various rotation rates, and corresponding Kouteck–Levich plots (inset).

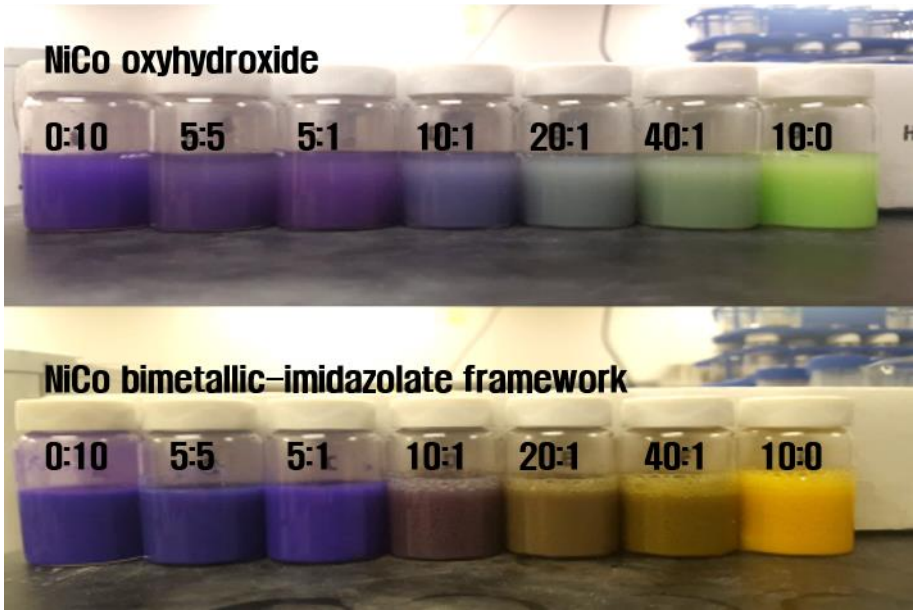

Figure S33. Pictures of nickel-cobalt hydroxide solutions synthesized at 90 ºC at 12 h with various molar ratio of nickel to cobalt as displayed (top) and nickel-cobalt bimetallic-imidazolate framework solutions(bottom) converted from nickel-cobalt hydroxide solutions at 40 ºC for 12 h.

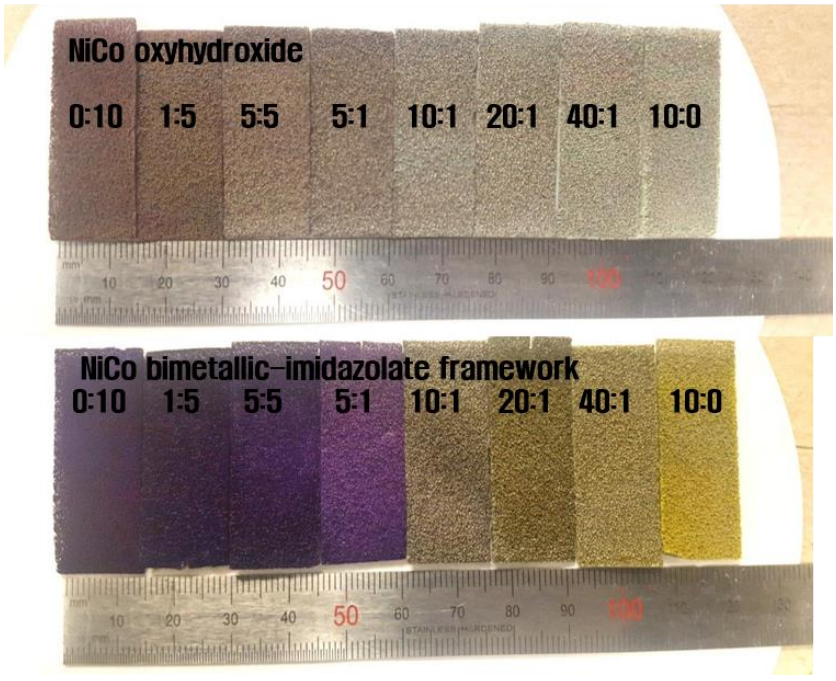

Figure S34. Pictures of nickel-cobalt hydroxide directly grown on nickel foam, synthesized at 90 ºC at 12 h with various molar ratio of nickel to cobalt as displayed (top) and nickel-cobalt bimetallic-imidazolate framework converted from nickel-cobalt hydroxide solutions at 40 ºC for 12 h (bottom).

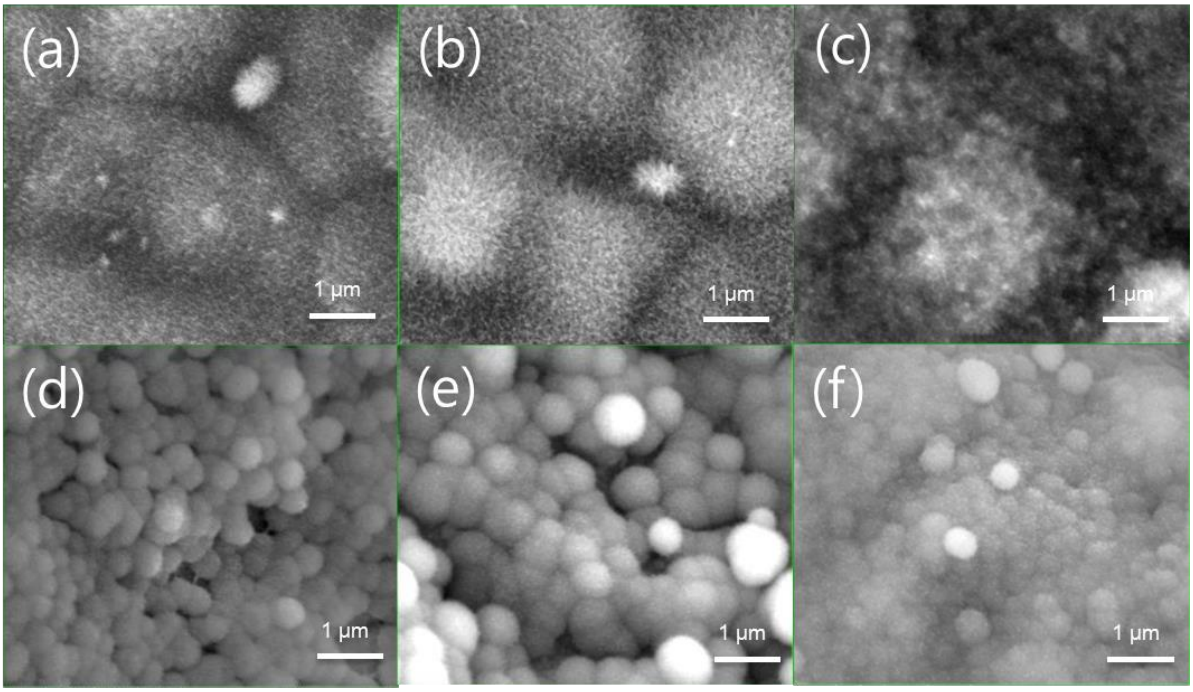

Figure S35. SEM images of nickel-cobalt hydroxide nanowires with a molar ratio of nickel to cobalt (a) 10:1, (b) 20:1, and (c) 0:10. All of the samples were synthesized at 90 ºC for 12 h. SEM images of bimetallic-imidazolate framework with a molar ratio of nickel to cobalt (d) 10:1, (e) 20:1, and (e) 0:10.

Table S1. Atomic ratio of each element in NiBMP@N_xC obtained from EDX, XPS, and IPC analyzes

Element	Determined by EDX	Determined by XPS	Determined by ICP
Ni	5.46	4.65	4.34
Co	2.16	1.66	1.63
P	8.86	6.60	-
N	3.68	3.22	-
C	47.98	54.21	-
O	31.86	29.66	-

Table S2. Comparison of the catalytic activities of NiBIF-derived catalysts with bi-functional catalysts for overall water splitting. The reference numbers are same as those in the main manuscript.

Catalyst	HER		OER		Overall water splitting		Ref.
	J (mA cm^{-2})	η (mV)	J (mA cm^{-2})	η (mV)	J (mA cm^{-2})	E (V)	
Co_xMo_y@NC	10	218	10	330	10	1.74	[45]
$NiMoP_2$	100	199	20 100	260 330	10	1.67	[46]
CoN/Ni_3N	10	68	10	247	10	1.56	[47]
NF@Ni/C-600	10 50	37 124	10 50	265 353	35.9	1.60	[17]
Cu@NiFe LDH catalysts	10 100	116 192	10 100	199 281	10 100	1.54 1.69	[43]
Cu@CoS_x/CF	10 100	134 267	10 100	160 310	10 100	1.50 1.80	[44]
NiBM@N_xC	20/100	71/134	20/100	194/310	-	-	This
NiBMP@N_xC	20/100	67/114	20/100	201/254	10/100	1.49/1.68	work

Table S3. Comparison of the catalytic activities of NiBIF-derived catalysts with bi-functional activity for metal-air batteries. The reference numbers are same as those in the main manuscript.

Catalyst	ORR		OER		Ref
	E_{onset} (mV)	$E_{1/2}$ (V)	J (mA cm^{-2})	η (mV)	
MnO@Co-N/C	-	0.83	10	530*	51
Fe@C-NG/NCNTs	0.93	0.84	10	450	52
CoNi@NCNT	0.97	0.87	10	310*	49
Co/Co_3O_4@PGS	-	0.89	10	350*	50
CoP NCs	0.92	0.858	10	330	25
Co_2P NCs	-	-	10	280	
NiBM@N_xC	0.98	0.88	20/100	71/134	This work
NiBMP@N_xC	0.92	0.82	20/100	67/114	

* OER activity was measured in 0.1 M KOH solution

Table S4. Comparison of the catalytic activities of NiBIF-derived catalysts with tri-functional activity. The reference numbers are same as those in the main manuscript.

Catalyst	HER		OER		ORR		Ref
	J (mA cm^{-2})	η (mV)	J (mA cm^{-2})	η (mV)	J (mA cm^{-2})	E (V)	
GO-PANi31-FP	10	~520 (0.1M)	10	~1.81	-	~0.71	[21]
Co0.85Se@NC	10	230	10	320	0.912	~0.81	[26]
Co/CoO@Co-N-C-800	20	436 (0.1M)	10	364 (0.1M)	0.914	0.78	[23]
defect-graphene	10	320	10	340	0.91	0.76	[22]
CoP NCs Co_2P NCs			10 10	330 280	0.92 -	0.858 -	[25]
NiBM@N_xC NiBMP@N_xC	20/100 20/100	71/134 67/114	20/100 20/100	194/310 201/254	- 10/100	- 1.49/1.68	This work